ISSN: 2688-8645

Research on Mechanical Properties of Variable Stiffness Self-Centering Three-Dimensional Seismic Isolators

Lianjie Ding

College of Civil Engineering, Henan Polytechnic University, Jiao Zuo, R.P.454000, China

Abstract

In order to improve the seismic performance of bridge structures, bridge isolation technology is increasingly innovating. However, current research is often limited by the contradiction between vertical bearing stiffness and seismic isolation performance: ensuring the daily operation of bridges requires high vertical stiffness load-bearing, while seismic isolation requires low dynamic stiffness. In response to this contradiction, this article proposes a Variable Stiffness Self centering Three dimensional Isolator (VSSC3DI), which consists of three parts: a vertical quasi zero stiffness isolation module and a lead core damper working together, and a combination system of friction pendulum and shape memory alloy (SMA) twisted wire in the horizontal direction. This article mainly studies the performance of vertical structures. By systematically explaining the working principle of the isolation device, constructing a static model and analyzing its force displacement relationship and the mechanism of quasi zero stiffness formation; Furthermore, the dynamic response of the system under external excitation was analyzed. Firstly, a corresponding nonlinear dynamic model was established, and the amplitude frequency response characteristics were solved using the averaging method. The excellent low-frequency isolation performance was confirmed through parameter analysis.

Keywords

Quasi Zero Stiffness; Variable Stiffness Mechanism; Nonlinear Dynamics; Low Frequency Shock Absorption.

1. Introduction

As the core hub of modern transportation networks, the seismic performance of bridge engineering is directly related to the social public safety system [1]. Therefore, it is crucial to implement effective seismic isolation measures for bridge structures. With the continuous development of bridge isolation technology, researchers have gradually realized that traditional isolation devices cannot simultaneously meet the high stiffness requirements during load-bearing and low stiffness requirements during isolation. In order to solve this contradiction, quasi zero stiffness isolation technology with "high static and low dynamic" stiffness characteristics has emerged [2].

In 1958, Molyneux et al. [3] optimized the structure of a positive stiffness elastic body; Subsequently, Alabuzhev et al. [4] introduced a negative stiffness device based on linear springs. Platus [5], Peng Xian [6-8], Lee et al. [9], Santillan et al. [10] designed various quasi zero stiffness systems by changing different negative stiffness mechanisms, and conducted nonlinear time history and energy analysis on them. Subsequently, Carrella et al. [11-12] designed a three spring quasi zero stiffness isolator, which provided an effective solution for low-frequency isolation.

The three spring structure quasi zero stiffness isolation device has shown significant advantages in the field of isolation. However, the quasi zero stiffness stroke of this structure is

ISSN: 2688-8645

relatively short, and the low-frequency isolation performance is limited. At present, the improvement of three types of spring quasi zero stiffness isolation devices mainly includes three aspects: optimizing damping characteristics, improving positive stiffness mechanisms, and innovating negative stiffness mechanisms. The design of negative stiffness mechanisms is the core of research on quasi zero stiffness isolators. In recent years, scholars have proposed various new negative stiffness mechanisms. For example, Huang and Liu et al. [13] designed an ultra-low frequency nonlinear isolation system composed of a sliding negative stiffness mechanism parallel to the vertical mechanical spring, and Yang et al. [14] also studied the dynamic behavior of nonlinear isolation systems with negative stiffness mechanisms. WS et al. [15] first proposed the use of magnetic springs to design quasi zero stiffness systems and verified their low-frequency seismic isolation performance through experiments. The results indicate that these improved quasi zero stiffness isolators can achieve a larger isolation range than ordinary three spring quasi zero stiffness isolators while maintaining ultra-low system stiffness and load-bearing capacity.

The variable stiffness self resetting three-dimensional seismic isolator proposed in this article achieves optimized design of negative stiffness in vertical structures by introducing a combination of transverse pre compressed coil springs and segmented nonlinear tracks, thereby ensuring significant improvement in seismic isolation performance while maintaining vertical bearing capacity.Through theoretical analysis, a mechanical model of VSSC3DI was established, and the force displacement and stiffness displacement equations of the system were derived. Based on the established mechanical model, the dynamic equations of the VSSC3DI system were further derived, and the second-order nonlinear differential equations were solved using the averaging method to obtain the amplitude frequency response equation and force transmission rate equation of the system. Parameterized research was conducted on the amplitude frequency response and force transmission rate characteristics of the system.

2. Static Performance Analysis of VCSS3DI

2.1. Structure of VSSC3DI

The vertical structure of VSSC3DI proposed in this article is shown in Figure 1, mainly composed of two parts: positive stiffness and negative stiffness. Negative stiffness is composed of segmented nonlinear guide rails, intermediate support blocks, anti pull stop blocks, horizontal preloading springs, sliders, and actuating rods, while positive stiffness is composed of lead core dampers and vertical disc spring groups

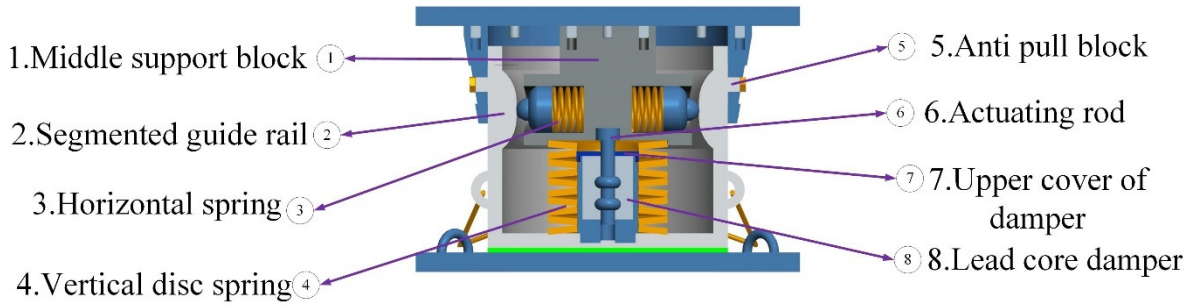

Fig 1. Structure of VSSC3DI

2.2. Working Principle of VSSC3DI

The overall stiffness of the classic three spring quasi zero stiffness isolation device consists of two parts: positive stiffness and negative stiffness. As in Figure2(a), positive stiffness is provided by linear springs, and negative stiffness is provided by transverse springs. Therefore, it can be designed to exhibit zero stiffness at the equilibrium position. However, when the

ISSN: 2688-8645

isolator is subjected to static loads or small deformations, this design may lead to issues of low stiffness and weak load-bearing capacity. The vertical mechanism of the seismic isolator proposed in this article can improve this situation through reasonable design. As shown in Figure2(b), the force displacement relationship of the seismic isolator exhibits a variable stiffness characteristic of "high low high" in the vertical direction through the influence of segmented nonlinear tracks and horizontal spring groups. This characteristic enables the seismic isolator to maintain low stiffness over a wide range of displacements, while also having good load-bearing capacity over a small displacement range.

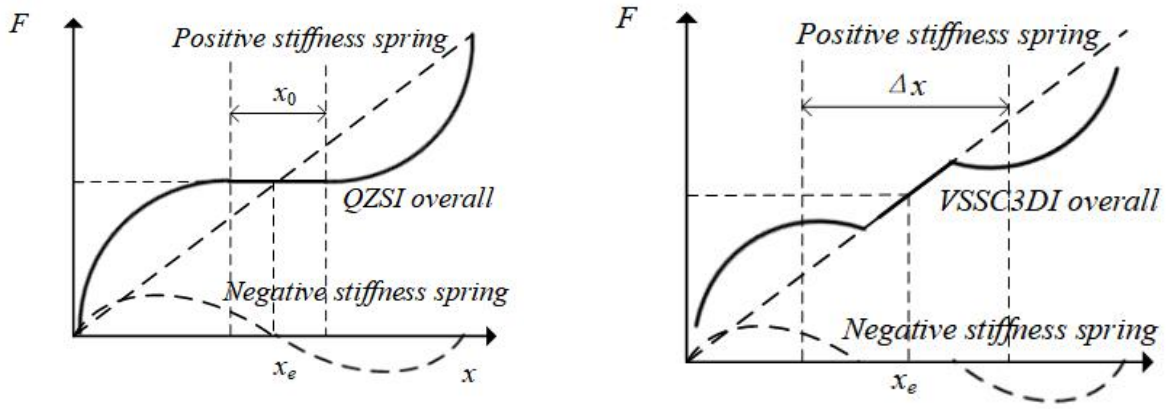

(a)QZSI (b)VSSC3DI

Fig 2. Composition of force displacement relationship between QZSI and VSSC3DI

2.3. Static Characteristics of VSSC3DI

2.3.1. VSSC3DI Mechanical Model

Figure 3 shows a simplified mechanical model under the action of the isolated object M, where R is the radius of the curved track and l_0 is the length of the vertical end track, k_h is the stiffness of the pre compressed disc spring in the horizontal direction, δ_h is its compression amount in the horizontal position, k_v is the stiffness of the vertical linear spring, δ_v is the compression of the vertical linear spring of the isolated object M in the horizontal direction, $\alpha=k_h/k_v$, let the friction coefficient of sliding on the guide rail be μ. In this state, the isolated object is only subjected to the restoring force generated by the vertical spring compression, that is, $mg = \delta_v k_v$. This component has been balanced, so there is no need to consider it again when deriving the force displacement relationship below.

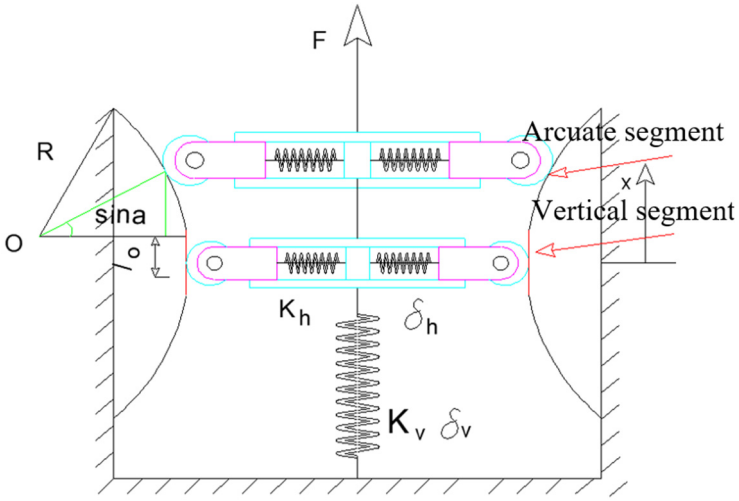

Fig 3. VSSC3DI Mechanical Model

ISSN: 2688-8645

Due to the fact that the direction of frictional force changes when the slider moves along a segmented nonlinear track, and the horizontal pre compression spring can only generate vertical force in the arc segment, segmented analysis is necessary.

According to the mechanical model shown in Figure 3, the force displacement relationship and geometric relationship of the system can be obtained:

$$F_{\mathrm{v}} = k_{\mathrm{v}} x \tag{1a}$$

$$F_{\mathrm{h}} = 2k_{\mathrm{h}}(\delta_{\mathrm{h}} - (R - \sqrt{R^2 - (x - \frac{l_0}{2})^2}))(\frac{1}{R}(x - \frac{l_0}{2})) \tag{1b}$$

$$F_{\mu} = 2\mu k_{\mathrm{h}}(\delta_{\mathrm{h}} - (R - \sqrt{R^2 - (x - \frac{l_0}{2})^2}))(\frac{1}{R}\sqrt{R^2 - (x - \frac{l_0}{2})^2}) \tag{1c}$$

When the slider is displaced $0 \le x \le x_{\max}$ along the guide rail, the restoring force model of the isolator:

$$F_{\mathrm{l1}} = \begin{cases} F_{\mathrm{v}} - F_{\mathrm{h}} + F_{\mu} & (x \cdot \dot{x} > 0) \\ F_{\mathrm{v}} - F_{\mathrm{h}} - F_{\mu} & (x \cdot \dot{x} < 0) \end{cases} \tag{1d}$$

$$F_{\mathrm{n1}} = \begin{cases} k_{\mathrm{v}} x + 2\mu k_{\mathrm{h}} \delta_{\mathrm{h}} & (x \cdot \dot{x} > 0) \\ k_{\mathrm{v}} x - 2\mu k_{\mathrm{h}} \delta_{\mathrm{h}} & (x \cdot \dot{x} < 0) \end{cases} \tag{1e}$$

When the slider moves $-x_{\max} \le x \le 0$ along the guide rail, due to the symmetry of the structure, there are:

$$F_{\mathrm{l2}}(x) = -F_{\mathrm{l1}}(-x) \tag{1f}$$

$$F_{\mathrm{n2}}(x) = -F_{\mathrm{n1}}(-x) \tag{1g}$$

Among them: F_{v} is the restoring force provided by a vertical linear spring, F_{h} is the restoring force provided by the horizontal pre compressed disc spring, F_{μ} is the frictional force experienced by the slider when it moves along the track, F_{11} is the overall restoring force of the slider when sliding on the upper curved track, F_{12} is the overall restoring force of the slider when sliding on the lower curved track, F_{n1} and F_{n2} is the overall restoring force of the slider when sliding on the upper and lower halves of the vertical track.

Organize formula (1) and make it $\bar{x}=x/\mathrm{R}, \alpha = k_{\mathrm{h}}/h_{\mathrm{v}}, \eta = l_0/2R$, $\gamma = \delta_{\mathrm{h}}/R$, $f_{\mathrm{v}} = F_{\mathrm{v}}/k_{\mathrm{v}}\mathrm{R}$, $f_{\mathrm{h}} = F_{\mathrm{h}}/k_{\mathrm{v}}\mathrm{R}, f_{\mu} = F_{\mu}/k_{\mathrm{v}}\mathrm{R}$, It can be organized into the following dimensionless form:

$$f_{\mathrm{v}} = \bar{x} \tag{2a}$$

$$f_{\mathrm{h}} = 2\alpha(\bar{x} - \eta)(\gamma - 1 + \sqrt{1 - \bar{x}^2 - \eta^2 + 2\eta\bar{x}}) \tag{2b}$$

$$f_{\mu} = 2\alpha\mu\sqrt{1 - \bar{x}^2 - \eta^2 + 2\bar{x}\eta}(\gamma - 1 + \sqrt{(1 - \bar{x}^2 - \eta^2 + 2\bar{x}\eta)}) \tag{2c}$$

$$f_{11} = \begin{cases} f_{\mathrm{v}} - f_{\mathrm{h}} + f_{\mu} & (\bar{x} \cdot \dot{\bar{x}} > 0) \\ f_{\mathrm{v}} - f_{\mathrm{h}} - f_{\mu} & (\bar{x} \cdot \dot{\bar{x}} < 0) \end{cases} \tag{2d}$$

$$f_{\mathrm{n1}} = \begin{cases} \bar{x} + 2\alpha\mu\gamma & (\bar{x} \cdot \dot{\bar{x}} > 0) \\ \bar{x} - 2\alpha\mu\gamma & (\bar{x} \cdot \dot{\bar{x}} < 0) \end{cases} \tag{2e}$$

$$f_{12}(\bar{x}) = -f_{11}(-\bar{x}) \tag{2f}$$

$$f_{\mathrm{n2}}(\bar{x}) = -f_{\mathrm{n1}}(-\bar{x}) \tag{2g}$$

Above $f_{11}, f_{\mathrm{n1}}, f_{\mathrm{n2}}, f_{12}$ is the restoring force of the seismic isolator during the sliding process of the slider.

ISSN: 2688-8645

2.3.2. Quasi Zero Stiffness Condition

According to the structure of the isolator, when the slider is located at the transition position between the vertical section and the curved section of the guide rail, the total stiffness of the system is zero. At this point, the nonlinear component of the transverse preloading spring and the linear stiffness of the vertical linear spring cancel each other out. Therefore, when $x=\pm\ \eta$, the stiffness is zero. By taking the derivative of equation (2d) and substituting it into the above conditions, we can obtain:

$$k_{xe}=1-2\alpha_{QZS}\gamma_{QZS}=0 \tag{3}$$

The value of α for the system under quasi zero stiffness conditions can be obtained from the above equation:

$$\alpha_{QZS}=\frac{1}{2\gamma} \tag{4}$$

2.3.3. Comparison of Static Characteristics between VSSC3DI and QZSI

In section 2.3.2 of the previous text, based on the quasi zero stiffness condition, the necessary conditions for the system to achieve total stiffness at a specific position were analyzed. This condition indicates that the total stiffness of the system is closely related to the parameters α and γ. Therefore, when conducting parameter analysis, the condition of stiffness ratio α=1 was selected to satisfy equation (4). In order to further explore the differences in force displacement and stiffness displacement characteristics between two types of seismic isolators, a set of parameters was selected for comparative analysis: friction coefficient μ=0.2, vertical segment ratio $\eta=0.2$. Through numerical calculations, the force displacement and stiffness displacement curves of two types of seismic isolators were obtained, as shown in Figure 4.

From the comparison of force displacement curves in Figure 4 (a), it can be seen that there are significant differences in the performance of VSSC3DI and QZSI isolators in different displacement ranges. In the small displacement stage, the force displacement curve shows a linear and rapid upward trend, and the growth rate is significantly higher than that of QZSI. This characteristic indicates that VSSC3DI has a high initial stiffness under small deformations, which helps to enhance the bearing capacity of the seismic isolator under static loads or small amplitude vibrations. However, when the slider entered the curved track stage, the force displacement relationship curve of VSSC3DI showed a significant decline and then continued to grow, but at a slower rate than QZSI. In addition, the curve of VSSC3DI also exhibits a certain hysteresis area in the latter half of the displacement, which is mainly attributed to the influence of friction during the movement of the slider, indicating that it not only has self resetting performance, but also has a certain energy dissipation ability. The analysis of the stiffness displacement curve in Figure 4 (b) is consistent with the force displacement relationship.

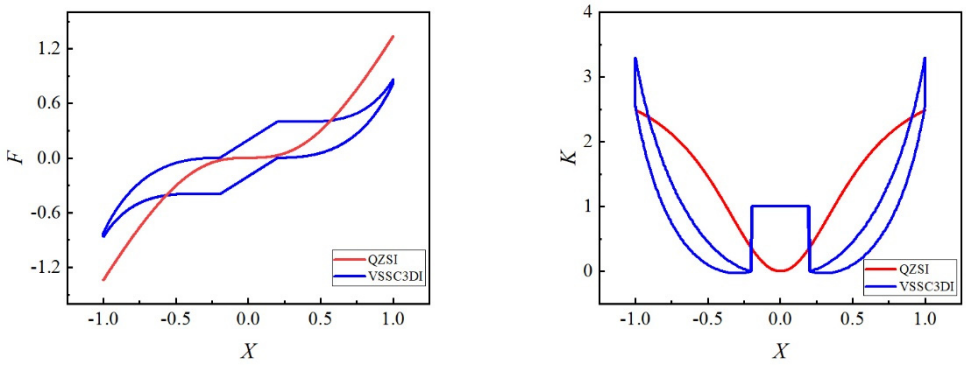

(a) Force displacement relationship (b) stiffness displacement relationship

Fig 4. Comparison of Static Characteristics between VSSC3DI and QZSI

ISSN: 2688-8645

3. Dynamic Performance Analysis of VSSC3DI

3.1. Establishment of VSSC3DI Dynamic Model

The dynamic model of the VSSC3DI single degree of freedom system studied in this article is shown in Figure 5.

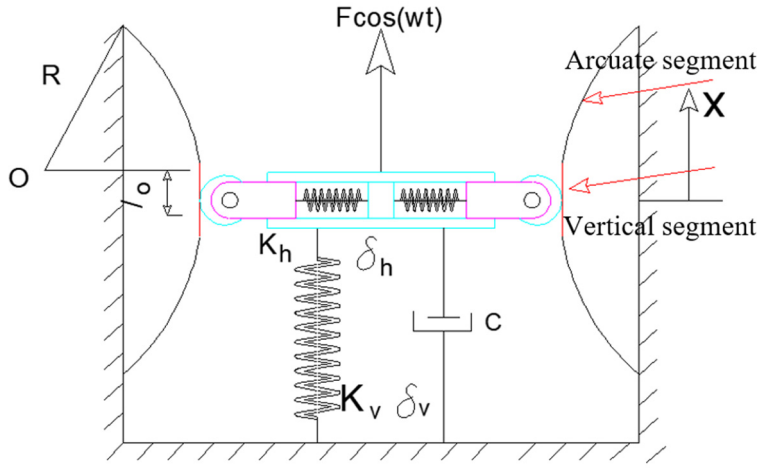

Fig 5. VSSC3DI dynamic model

According to the mechanical model shown, combined with the d'Alembert principle, the dynamic equation of the system can be obtained as follows:

When the slider moves $0 \le x \le x_{max}$ along the guide rail:

$$m\ddot{x} + c\dot{x} + F_{l1} = F\cos\omega t \tag{5a}$$

$$m\ddot{x} + c\dot{x} + F_{n1} = F\cos\omega t \tag{5b}$$

When the slider moves $-x_{max} \le x \le 0$ along the guide rail:

$$m\ddot{x} + c\dot{x} + F_{l2} = F\cos\omega t \tag{5c}$$

$$m\ddot{x} + c\dot{x} + F_{n2} = F\cos\omega t \tag{5d}$$

Among them: F_{11}, F_{12}, F_{n1} and F_{n2} have been given earlier and will not be further elaborated here. M is the mass of the isolated object, c is damping, F is the applied external excitation force, and ω is the applied excitation frequency. Let $\omega_0 = \sqrt{k_v/m}$, $\zeta = c/2m\omega_0$, $f_{11} = F_{11}/k_vR$, $f_{n1}=F_{n1}/k_vR$, $f_{12}=F_{12}/k_vR$, $f_{n2}=F_{n2}/k_vR$, $f=F/k_vR$, $\tau=\omega_0 t$, $\lambda=\omega/\omega_0$,, nondimensionalize equation (8) and add $\omega^2=\omega_0^2(1+\varepsilon\sigma_1)$ to the left and right of the equation in order to satisfy the mean method, ω_0 is the natural frequency of the system, organized as follows:

When the slider moves $0 \le \bar{x} \le \bar{x}_{max}$ along the guide rail:

$$\ddot{\bar{x}}_{l1} + \lambda^2\bar{x} = -2\zeta\dot{\bar{x}} - f_{l1} + f\cos\lambda\tau + (1+\varepsilon\sigma_1)\bar{x} \tag{6a}$$

$$\ddot{\bar{x}}_{n1} + \lambda^2\bar{x} = -2\zeta\dot{\bar{x}} - f_{n1} + f\cos\lambda\tau + (1+\varepsilon\sigma_1)\bar{x} \tag{6b}$$

When the slider moves $-\bar{x}_{max} \le \bar{x} \le 0$ along the guide rail:

$$\ddot{\bar{x}}_{l2} + \lambda^2\bar{x} = -2\zeta\dot{\bar{x}} - f_{l2} + f\cos\lambda\tau + (1+\varepsilon\sigma_1)\bar{x} \tag{6c}$$

$$\ddot{\bar{x}}_{n2} + \lambda^2\bar{x} = -2\zeta\dot{\bar{x}} - f_{n2} + f\cos\lambda\tau + (1+\varepsilon\sigma_1)\bar{x} \tag{6d}$$

To obtain an approximate solution for the system, Taylor series expansion can be performed on the relevant variables near the upper and lower endpoints of the arc and vertical segments. Right to f_{11} and f_{12} in f_μ and f_h is expanded at $\bar{x}=\pm\eta$ as follows:

ISSN: 2688-8645

At $\bar{x}=\eta$:

$$\begin{cases} f_{\mathrm{h}} = -2\alpha\gamma(\eta-\bar{x}) + \alpha(\eta-\bar{x})^3 \\ f_{\mu} = 2\alpha\gamma\mu - 2\alpha\mu(\frac{\gamma}{2}+\frac{1}{4})(\eta-\bar{x})^2 \end{cases} \tag{7a}$$

At $\bar{x}=-\eta$:

$$\begin{cases} f_{\mathrm{h}}(\bar{x}) = -f_{\mathrm{h}}(-\bar{x}) \\ f_{\mu}(\bar{x}) = -f_{\mu}(-\bar{x}) \end{cases} \tag{7b}$$

3.2. Average Method for Solving

Let the main resonance response of the system be solved as:

$$\bar{x} = A\cos(\lambda\tau+\varphi) \tag{8}$$

Among them :A Expressing amplitude, φ indicates phase difference. Order $\Phi = \lambda\tau+\varphi$,according to the average method, solve as follows:

$$\frac{\mathrm{d}A}{\mathrm{d}\tau} = -\frac{\int_0^{2\pi}[2\zeta A\lambda\sin\Phi + f\cos\lambda\tau + (1+\varepsilon\sigma_1)A\cos\Phi - Y]\sin\Phi\mathrm{d}\Phi}{2\pi\lambda} \tag{9a}$$

$$\frac{\mathrm{d}\varphi}{\mathrm{d}\tau} = \frac{\int_0^{2\pi}[2\zeta A\lambda\sin\Phi + f\cos\lambda\tau + (1+\varepsilon\sigma_1)A\cos\Phi - Y]\cos\Phi\mathrm{d}\Phi}{2A\pi\lambda} \tag{9b}$$

Among them, Y represents the dimensionless overall restoring force of the isolation device at different stages, that is, f_{11},f_{12},f_{n1},f_{n2}

Solve equation (9) simultaneously, and let $\frac{\mathrm{d}A}{\mathrm{d}\tau}=\frac{\mathrm{d}\varphi}{\mathrm{d}\tau}=0$,The amplitude frequency response equation can be obtained:

$$\begin{cases} 2\zeta A\lambda + B_{\mathrm{A}} = f\sin\varphi \\ B_{\varphi} + A - A\lambda^2 = f\cos\varphi \end{cases} \tag{10}$$

The amplitude frequency response equation of the system can be solved by the equation system (10), namely:

$$\left(B_{\varphi}+A-A\lambda^2\right)^2 + \left(2\xi A\lambda + B_{\mathrm{A}}\right)^2 = f^2 \tag{11}$$

Equation (11) can be used to calculate the force transmission rateT_{F}, the force transmission rate is determined as the maximum value of the response transmitted to the base F_{T} to the maximum value of motivation f:

$$T_{\mathrm{F}} = \left|\frac{F_{\mathrm{T}}}{f}\right| = \sqrt{\frac{\left(B_{\varphi}+A\right)^2 + \left(2\xi A\lambda + B_{\mathrm{A}}\right)^2}{f^2}} \tag{12}$$

Among them :

$$B_{\mathrm{A}} = \begin{cases} B_{\mathrm{A1}}, 0 \le A \le \eta \\ B_{\mathrm{A2}}, \eta \le A \end{cases}$$

$$B_{\mathrm{A1}} = 0,\quad B_{\mathrm{A2}} = \frac{4(2\alpha\gamma\mu - \frac{\alpha\mu\eta^2}{2} - \alpha\gamma\mu\eta^2)(1-\cos(\arccos(\frac{\eta}{A})))}{\pi} + \frac{4A(\alpha\eta\mu + 2\alpha\gamma\mu\eta)(\frac{\sin(\arccos(\frac{\eta}{A}))^2}{2})}{\pi}$$

$$+ \frac{4A^2(-\frac{\alpha\mu}{2} - \alpha\gamma\mu)(\frac{1}{3} - \frac{\cos(\arccos(\frac{\eta}{A}))^3}{3})}{\pi}$$

ISSN: 2688-8645

$$B_{\varphi}=\begin{cases}B_{\varphi 1}, 0\le A\le \eta\\ B_{\varphi 2}, \eta\le A\end{cases}$$

$$B_{\varphi 1}=0$$

$$B_{\varphi 2}=\frac{-4(\alpha\eta^3-2\alpha\gamma\eta)(\sin(\arccos(\frac{\eta}{A})))}{\pi}-\frac{A(2\alpha\gamma-3\alpha\eta^2)(\sin(2\arccos(\frac{\eta}{A})+2\arccos(\frac{\eta}{A})))}{\pi}$$
$$-\frac{12A^2\alpha\eta(\sin(\arccos(\frac{\eta}{A}))-\frac{\sin(\arccos(\frac{\eta}{A}))^3}{3})}{\pi}$$
$$+\frac{4A^3\alpha(\frac{\sin(2\arccos(\frac{\eta}{A}))}{4}+\frac{\sin(4\arccos(\frac{\eta}{A}))}{32}+\frac{3\arccos(\frac{\eta}{A})}{8})}{\pi}$$

3.3. Comparison of Dynamic Characteristics between VSSC3DI,,QZSI, and Linear Systems

Figure 6 shows the amplitude frequency response curves of QZSI and linear systems plotted under the conditions of damping ratio $\zeta = 0.02$ and dimensionless excitation amplitude $f = 0.02$. For the VCSS3DI system, the amplitude frequency response stress and force transfer rate curves were obtained by taking the friction coefficient $\mu = 0.1$ and the vertical end ratio $\eta = 0.1$.

From Figure 6 (a), it can be seen that the amplitude frequency curve of the VSSC3DI system shows a leftward bending trend within larger amplitudes, indicating that its peak response is significantly lower than that of the QZSI system and its corresponding linear system. As can be seen from Figure 6 (b), The force transmission rate curve of the VSSC3DI system is significantly lower at the peak than that of the QZSI system and linear system, indicating that the VSSC3DI system can effectively reduce the force transmitted to the structure, fully demonstrating its excellent seismic isolation performance.

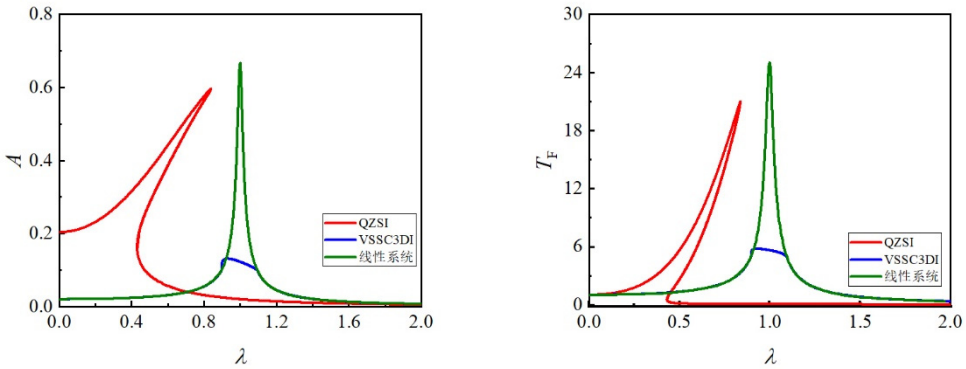

(a)amplitude frequency response (b)force transmissibility

Fig 6. QZSI, Comparison of dynamic characteristics between VSSC3DI and linear systems

3.4. Effects of Different Parameters on System Dynamics Performance

As shown in Figure 7, under the conditions of $\zeta = 0.05$,$\mu = 0.2$,$\eta = 0.2$, changing the excitation amplitude has a significant impact on the amplitude frequency response curve and force transmission rate curve. As the excitation amplitude gradually increases, the system response curve exhibits obvious nonlinear characteristics, manifested as an overall leftward shift of the curve, indicating that the resonance frequency of the system decreases with the increase of

ISSN: 2688-8645

excitation amplitude. At the same time, the overall force transmission rate curve bends to the lower left, showing a decrease in resonance peak and a corresponding decrease in resonance frequency

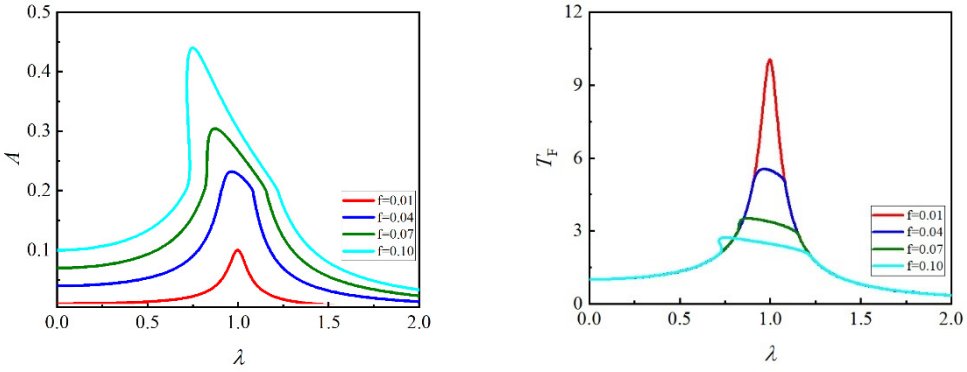

(a)amplitude frequency response (b)force transmissibility

Fig 7. The influence of different f on the dynamic performance of the system

Figure 8 shows the effect of changing the parameter ζ on the amplitude frequency response curve and force transmission rate at $f = 0.04, \mu = 0.2, \eta = 0.2$.From the graph, it can be seen that as the damping ratio ζ gradually increases, the trend of the amplitude frequency response curve of the system bending to the left in the low-frequency region gradually decreases, manifested as a gradual decrease in the peak value, and the corresponding peak frequency also increases, gradually approaching the resonance frequency of the linear system. In the high-frequency region, the impact is relatively small, and as the damping ratio increases, the system begins to exhibit linear characteristics. Meanwhile, as the damping ratio increases, the law of force transmission rate and amplitude frequency response curve remains consistent, and the peak gradually decreases. Reasonable selection of damping ratio can optimize the seismic isolation performance while ensuring system stability.

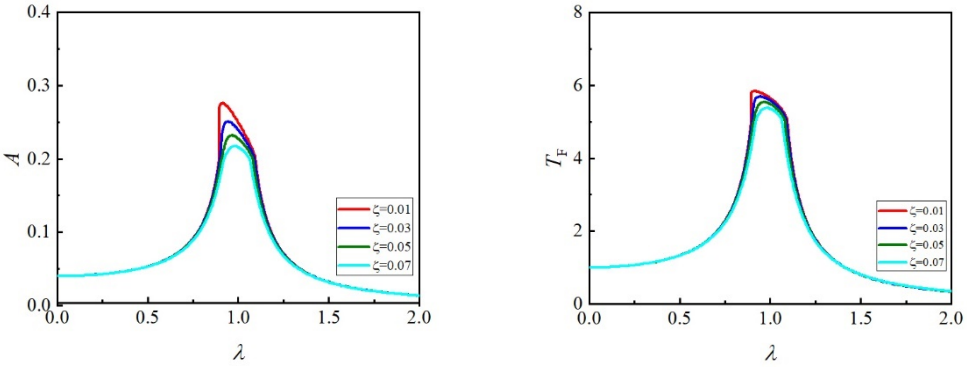

(a)amplitude frequency response (b)force transmissibility

Fig 8. The influence of different ζ on the dynamic performance of the system

Figure 9 shows the effect of changing the parameter η on the amplitude frequency response and force transmission rate curves at $f = 0.04, \mu = 0.2, \zeta = 0.05$. From the graph, it can be seen that in areas with relatively low or high frequencies, the variation in the proportion of vertical segments has a relatively small impact on the amplitude frequency response curve. In the resonance region with a frequency ratio close to 1, as the proportion of vertical segments decreases, the amplitude frequency response curve of the system shows a leftward bending trend, indicating that the resonance frequency of the system decreases, and the peak amplitude also significantly decreases. At the same time, the force transmission rate curve shifts to the left as a whole in the curve with a frequency ratio close to 1, and the peak value significantly

ISSN: 2688-8645

decreases. This indicates that reducing the proportion of vertical segments can effectively reduce the vibration amplitude of the system in the resonance region, reduce energy transfer, and improve the overall seismic isolation effect of the system.

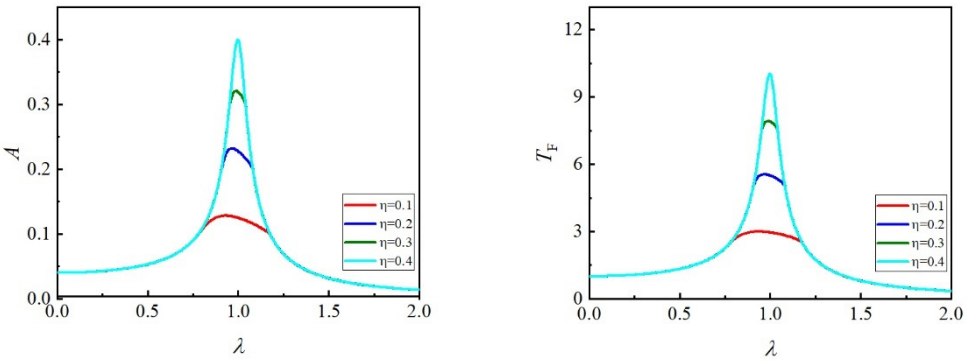

(a)amplitude frequency response (b)force transmissibility

Fig 9. The influence of different η on the dynamic performance of the system

Figure 10 shows the effects of changing the parameter μ on the amplitude frequency response and force transfer rate curves at$\eta = 0.2, \zeta = 0.05, f = 0.04$, respectively. From the graph, it can be seen that when the friction coefficient is low, as the friction coefficient increases, the peak values of the system's amplitude frequency response curve and force transmission rate rapidly decrease. In the high friction coefficient region, the effect of increasing the friction coefficient on the amplitude frequency response curve and force transmission rate curve tends to stabilize, and the peak change is not significant.

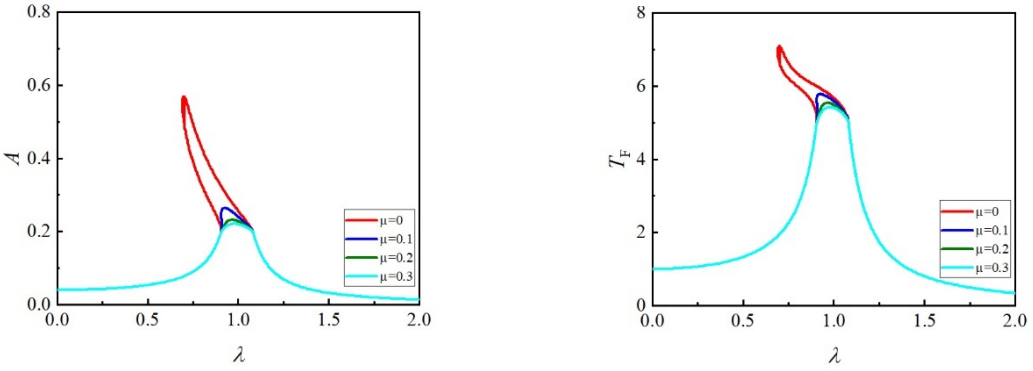

(a)amplitude frequency response (b)force transmissibility

Fig10. The influence of different μ on the dynamic performance of the system

4. Conclusion

This article proposes a three-dimensional seismic isolator based on a variable stiffness self resetting mechanism, which vertically utilizes the high static and low dynamic characteristics of the quasi zero stiffness isolator, replaces the negative stiffness spring in the classical three springs with segmented nonlinear tracks, transverse disc springs, and sliders, so that the isolator has a high low high stiffness characteristic when subjected to external excitation in the vertical direction, effectively balancing the contradictory relationship between bearing capacity and isolation performance. Next, establish the static and dynamic models of the isolation device, derive the force displacement equation, amplitude frequency response, and force transfer rate equation, and then study the influence of structural parameter changes on the performance of the isolation device. Draw the following conclusion:

ISSN: 2688-8645

(1) Static characteristic analysis was conducted on VCSS3DI, and equations for force displacement and stiffness displacement were obtained. The quasi zero stiffness condition was determined and compared with the classical three spring quasi zero stiffness isolation device. The results indicate that compared with the QZSI system, the VCSS3DI system has greater stiffness under small displacements, which helps to improve the bearing capacity of the seismic isolator under static loads or small deformations.

(2) The dynamic characteristics of the VCSS3DI system were analyzed and compared with linear isolators and classical three spring quasi zero stiffness isolators. The results showed that compared with the QZSI system and the corresponding linear system, the resonance amplitude in the amplitude frequency response and force transmission rate of the VCSS3DI system decreased, indicating that the force transmitted to the structure was smaller, further verifying the good low-frequency vibration isolation performance of VCSS3DI.

References

[1] Guo W. Research on Seismic Performance Evaluation and Reinforcement Technology of Highway Bridges [J], 2023.

[2] Jing X,Yu W,Li Q. Design of a quasi-zero-stiffness based sensor system for the measurement of absolute vibration displacement of moving platforms[J], 2016.

[3] Molyneux,W. G. The Support of an Aircraft for Ground Resonance Tests: A Survey of Available Methods[J], 1958.

[4] Alabuzhev PM,Rivin EI. Vibration protecting and measuring systems with quasi-zero stiffness[J].

[5] Platus DL. Negative-stiffness-mechanism vibration isolation systems[J], 1999.

[6] Peng X. Static and linear dynamic characteristics analysis of a quasi zero stiffness isolation system [J]. Chinese Quarterly of Mechanics, 2012, 33(03): 492-498.

[7] Peng X, Cheng SN. Preliminary exploration of the working principle and application of negative stiffness [J]. Journal of Hunan University (Natural Sciences), 1992, (04): 89-94.

[8] Peng X, Cheng SN. Design of quasi zero stiffness isolator and its elastic characteristics [J]. Journal of Vibration, Measurement &Diagnosis, 1997, (04): 44-46.

[9] Lee CM,Goverdovskiy VN,Samoilenko SB. Prediction of non-chaotic motion of the elastic system with small stiffness[J], 2004.

[10] Virgin LN,Santillan ST,Plaut RH. Vibration isolation using extreme geometric nonlinearity[J], 2008.

[11] Carrella A,Brennan MJ,Waters TP. Static analysis of a passive vibration isolator with quasi-zero-stiffness characteristic[J], 2007.

[12] Carrella A,Brennan MJ,Waters TP. On the design of a high-static-low-dynamic stiffness isolator using linear mechanical springs and magnets. [In special Issue: EUROMECH colloquium 483, Geometrically non-linear vibrations of structures] [J], 2008.

[13] Huang X,Liu X,Hua H. On the characteristics of an ultra-low frequency nonlinear isolator using sliding beam as negative stiffness[J], 2014.

[14] Yang J,Xiong YP, Xing JT. Dynamics and power flow behaviour of a nonlinear vibration isolation system with a negative stiffness mechanism[J], 2013.

[15] Robertson WS, Cazzolato BS, Zander AC. Nonlinear control of a one axis magnetic spring[J], 2007.